IMPACT OF BROKEN AND INHOMOGENEOUS CLOUDS ON SATELLITE CLOUD-PHASE RETRIEVAL

E.L.A. Wolters[*], H.M. Deneke[+], J.F. Meirink[*], and R.A. Roebeling[*]

[*]: Royal Netherlands Meteorological Institute, P.O. Box 201, 3730 AE De Bilt, The Netherlands
[+]: Meteorological Institute University of Bonn, Auf dem Hügel 20, 53121 Bonn, Germany.

Abstract

The influence of broken and inhomogeneous clouds on satellite cloud-phase retrievals is investigated. The research comprises two parts: First, an assessment of the effect of broken and inhomogeneous water clouds on the cloud-phase retrieval is performed through an evaluation of the errors in retrieved optical thickness (τ) and effective radius (r_{eff}) using synthetic datasets. Second, a comparison of MODIS low-resolution (3x3 km) cloud properties against corresponding high-resolution (1x1 km) retrievals for low-resolution cases of broken and inhomogeneous clouds was carried out. The evaluation of the synthetic datasets reveal that, for water clouds with high values of τ and r_{eff}, a shift in cloud phase from 'water' to 'ice' can be expected at cloud fractions between 0.4 and 0.8. For overcast fields of inhomogeneous water clouds, r_{eff} is overestimated by ~3-5 μm at low-resolution as compared to high-resolution. Depending on the amount of cloud variability and the underlying surface this overestimation may lead to a shift in cloud phase from 'water' to 'ice'. Although the MODIS observations do not reveal a sharp increase in r_{eff} with decreasing cloud fraction, the expected increase in r_{eff} for inhomogeneous overcast water clouds is clearly manifested in the observations.

1. INTRODUCTION

Clouds strongly affect the Earth's surface energy budget by reflection and absorption of solar irradiance. The way in which this energy balance is modulated depends among others on the particle size distribution, height and thermodynamic phase of clouds. The reflection of incoming shortwave radiation is the dominating effect for water clouds, which generally cools the atmosphere. For ice clouds the absorption and remittance of outgoing terrestrial radiation back to the Earth's surface is the dominating effect, thereby causing a net warming. In spite of their importance, clouds are still treated in a simplified manner in climate models, which is partly due to the lack of knowledge of the spatial and temporal variations in cloud properties and partly because of the limitations imposed by computational resources.

Within the EUMETSAT Climate Monitoring Satellite Application Facility an algorithm is presented to discriminate water from ice clouds (CM-SAF, Schulz et al., 2008). This algorithm primarily uses visible (0.6 μm) and near-infrared (1.6 μm) observations from passive imagers, and was validated against ground-based cloud radar and lidar observations (Wolters et al., 2008). This paper addresses the question to what extent broken and inhomogeneous clouds influence cloud-phase retrieved from passive imagers at different spatial resolutions over different surfaces (ocean and mid-latitude land). To answer this question the work is performed in two parts. First, the impact of broken cloudiness on cloud phase retrieval is scrutinized by simulating the effect of these clouds on cloud optical thickness (τ) and effective radius (r_{eff}) retrievals. A similar investigation is done for overcast fields of water clouds, but then using different degrees of inhomogeneity. Second, the CM-SAF Cloud Physical Properties (CPP) retrieval algorithm is applied to measured reflectances and radiances from the Moderate Resolution Imaging Spectroradiometer (MODIS) onboard NASA's EOS *Terra* and *Aqua* satellites on both 1x1-km data and data averaged to the Spinning Enhanced Visible and Infrared Imager (SEVIRI)-like resolution (3x3 km). The observational datasets comprise two months of 2007.

The outline of the paper is as follows. In section 2, the MODIS datasets, the CPP algorithm, and the experimental set-up of the synthetic dataset evaluation are presented. The simulations and first results

for the MODIS cloud datasets obtained at different resolutions for the central European area are shown in section 3. Finally, in section 4 a summary is provided and conclusions are drawn.

2. DATA AND METHODS

2.1 MODIS data

The MODIS instrument onboard the NASA EOS Terra and Aqua satellites carry 36 onboard calibrated channels (0.42-14.2 μm). In this study the Level-1B (1x1 km) reflectance and radiance data from band 1 (0.65 μm), 6 (1.64 μm), and 31 (11.0 μm) are used. The cloud mask was extracted from corresponding MODIS Level-2 data (MOD035 product). This cloud mask is produced by the MODIS cloud/clear sky discrimination algorithm (Frey et al., 2008), which comprises a set of cloud spectral tests applied to 20 of the 36 available MODIS bands and generates four cloud probability categories, i.e. *confident clear*, *probably clear*, *probably cloudy* and *confident cloudy*, at both 1-km and 5-km resolution. Here we use the 1-km resolution cloud mask. Surface albedo information over land was obtained from 16-day MODIS white sky albedo maps, while over ocean an albedo of 0.05 was assumed for both the MODIS 0.65-μm and 1.64-μm channel. MODIS data with viewing (θ) and solar zenith angles (θ_o) larger than 60^o were excluded from this study because the cloud physical properties retrievals at such large θ and θ_o are known to be less accurate and precise (Roebeling et al., 2008; Wolters et al., 2008).

2.2. CPP retrieval algorithm

The cloud thermodynamic phase determination method used in this paper is part of the CPP algorithm developed at the Royal Netherlands Meteorological Institute (KNMI) within the framework of the CM-SAF. It primarily uses the visible (0.6 μm) and near-infrared (1.6 μm) spectral channel reflectances to retrieve τ, r_{eff}, and cloud thermodynamic phase. The algorithm is operationally applied to radiances observed from passive imagers, such as the SEVIRI or MODIS instruments.

τ and r_{eff} are derived simultaneously through comparison of the observed 0.6-μm and 1.6-μm reflectances with pre-calculated Radiative Transfer Model (RTM) lookup table (LUT) reflectances for given cloud optical thickness, particle effective radius, and surface albedo for water and ice clouds (Roebeling et al., 2006). The r_{eff} retrievals for clouds with $\tau < 8$ are relaxed to a climatological average of 8 μm, since the r_{eff} retrievals can become ambiguous for these clouds when using a two-channel algorithm (Nakajima and King, 1990). The phases “water” and “ice” are assigned to those pixels for which the measured 0.6-μm and 1.6-μm reflectances correspond to the simulated reflectances of these clouds. Since visual image inspection revealed that ice is erroneously assigned to optically thin water clouds (e.g. at the edges of cloud fields), a cloud-top temperature check based on measured 10.8-μm brightness temperature was included This check assigns the cloud-phase “water” to cloud pixels that are initially labelled “ice”, but have a cloud-top temperature warmer than 265 K. The 10.8-μm brightness temperatures are corrected for cloud emissivity using the relation between the cloud optical thickness at visible and thermal infrared wavelengths (Minnis et al., 1998).

The Doubling Adding KNMI (DAK, De Haan et al., 1987; Stammes, 2001) RTM is used to simulate cloud reflectances. In DAK, clouds are assumed to be plane parallel and homogeneous over a Lambertian surface. In the LUTs the optical thicknesses range from 1 to 256, while the particles of water clouds are assumed to be spherical droplets with effective radii between 1 and 24 μm. For ice clouds imperfect hexagonal ice crystals (Hess et al., 1998) are assumed with effective radii between 6 and 51 μm.

2.3. Analysis procedures

In order to obtain a first quantitative indication of the effect of broken and inhomogeneous clouds on cloud-phase retrievals, synthetic clouds fields at high (1x1 km) and low (3x3 km) resolution were compared for cases where these effects occurred. For clearness of presentation, the inhomogeneity effect is only investigated for overcast cloud scenes, although it is recognized that in reality broken cloud fields can be also inhomogeneous, such as in developing convection. Furthermore, it is stressed that 3D cloud effects were not taken into account. To determine the effect of broken and inhomogeneous clouds on the cloud-phase retrievals of true observations, two months MODIS cloud

property retrievals over land and ocean areas at high and low resolution are compared. Hereinafter we will refer to the low- and high-resolution simulations as LRES and HRES, respectively.

a) Broken cloud simulations

The synthetic broken water cloud fields were prepared for subsets of 100x100 pixels, with each pixel representing a 1x1 km HRES pixel. The superimposed LRES pixels were chosen to comprise 4x5 HRES pixels. τ and r_{eff} values of the synthetic clouds fields were fixed at τ = 8 and r_{eff} = 12 μm, representing a broken cloud field with thin clouds and at τ = 20, r_{eff} = 16 μm for a cloud field with thick broken clouds. The choice of these cloud fields was based on the MODIS high-resolution τ and r_{eff} observations presented in Figure 1b. The cloud fraction of the synthetic LRES pixels was simulated by assigning a value of τ = 0 to a number of HRES pixels, depending on the cloud free fraction. The simulated reflectances in the LUT are used to relate τ and r_{eff} to synthetic cloud reflectances at 0.6 and 1.6 μm. Note that at τ = 0 the 0.6 and 1.6 μm reflectances represent the clear sky reflectances over a typical ocean and mid-latitude land surface. The clear and cloudy reflectances were averaged over the 4x5 HRES pixels to acquire the LRES reflectance (representing a SEVIRI pixel), after which the CPP algorithm is used to retrieve τ and r_{eff} for the synthetic LRES cloud fields. The simulations were performed for $\theta=\theta_o=10^o$ and azimuth difference angle $\phi-\phi_o=100^o$.

b) Inhomogeneous overcast cloud simulations

The synthetic fields of inhomogeneous clouds were prepared for subsets of 100x100 pixels, which were completely overcast and comprise water clouds only. The degree of inhomogeneity was simulated by variation in τ, with r_{eff} kept constant, and is defined by the normalized interquartile range of τ, hereafter referred to as $NIQR_\tau$:

$$NIQR_\tau = \frac{\tau_{75} - \tau_{25}}{\tau_{50}},$$

where τ_{25}, τ_{50}, and τ_{75} denote the 25-, 50- and 75-percentile value of the τ distribution, respectively. In case of a homogeneous overcast cloud ($NIQR_\tau$=0), all HRES τ values were equal. For $NIQR_\tau > 0$, r_{eff} was still fixed at 12 µm or 16 μm, whereas τ values were randomly drawn from a lognormal distribution. The mean (μ) and standard deviation (σ) of the lognormal distribution were chosen such that $NIQR_\tau$ equalled 0.25, 0.50,..., 1.50. By only varying τ rather than also r_{eff}, we were able to clearly quantify the influence of HRES τ variability on the LRES r_{eff} retrieval, as a change in τ affects both the 0.6-µm and 1.6-µm reflectance, especially at low τ and r_{eff}. The averaging and retrieval procedure were carried out analogue to the broken cloud simulations.

c) Observational analysis procedure

The MODIS cloud property datasets were obtained for central Europe during May and August 2007. The cloud properties were retrieved from these datasets with a version of the algorithm that was developed for retrievals from MODIS reflectances. LRES retrievals were obtained from MODIS 1x1-km reflectances and surface albedo values which were averaged to the SEVIRI resolution. The HRES CPP retrievals were derived from the original 1x1-km MODIS reflectances, after which the retrieved values were averaged to LRES. Additional statistics on cloud fraction, the fraction of water and ice clouds, and variability in HRES cloud optical thickness were calculated. The statistics were only calculated if an LRES pixel contained at least 10 cloud flagged HRES pixels.

3. RESULTS

3.1 General

Figure 1a shows the LRES cloud fraction distribution as obtained from the MODIS observations for May and August 2007 over central Europe. In order to better focus on broken clouds, only cloud fractions between 0.02 and 0.98 are shown. Cloud free and overcast clouds contribute ~42% each to the total distribution, leaving ~15% for broken clouds. When only cloud flagged pixels are considered, about 25% of the LRES pixels represent broken clouds. The broken cloud cases are evenly distributed over cloud fractions between 0.02 and 0.98. The joint frequency distribution of HRES τ and r_{eff} is

shown in Figure 1b. The lognormal distribution for τ can be recognized from the higher frequencies at low τ. Further, it can clearly be seen that for optically thin clouds (τ <~4) the corresponding r_{eff} value is dominated by the climatological value of 8 μm, which is imposed by the CPP algorithm. At larger τ values, r_{eff} increases, although values rarely exceed 20 μm.

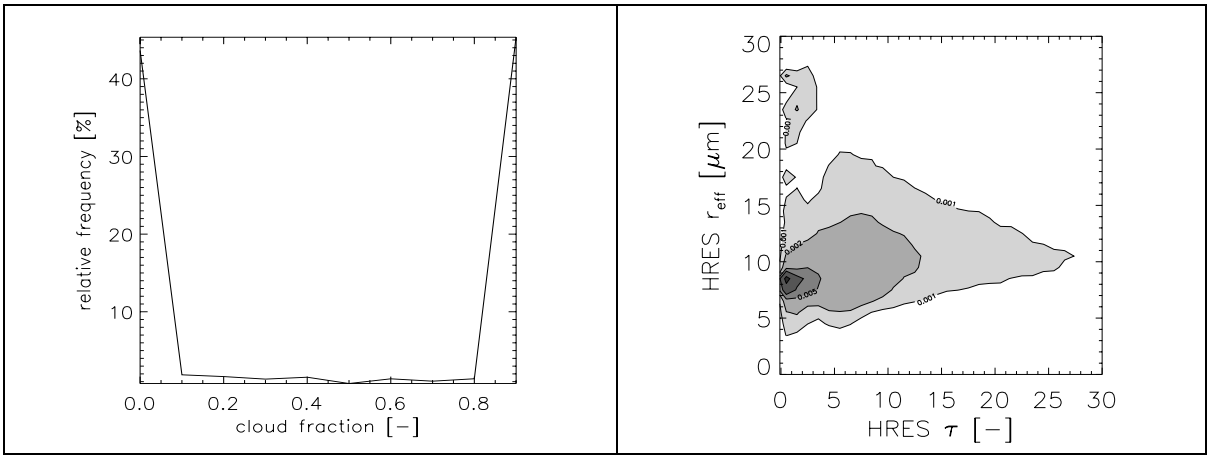

Figure 1 **a) Frequency distribution of LRES cloud fraction as obtained from 1x1-km MODIS Terra data over central Europe. The MODIS cloud mask was used for cloud screening, b) joint histogram of HRES τ vs r_{eff} obtained from MODIS 1x1-km data over the EUR area, with binsize=1.0 (μm) for both τ and r_{eff}, countour intervals are plotted at frequencies 0.001, 0.002, 0.005, 0.01, and 0.02.**

3.2. Broken cloud simulations

Figure 2 shows for simulated LRES water clouds the relationship between cloud fraction and τ (upper panels) and r_{eff} (lower panels) for an underlying dark (solid line) and bright surface (dashed line). The calculations in the left panels were done for HRES clouds with τ=8 and r_{eff}=12 μm, while the results in the right panels were done for HRES clouds with τ=20 and r_{eff}=16 μm. Figure 2a and 2b show that the τ values of the LRES pixels linearly increase with cloud fraction for both τ=8 and τ=20. The r_{eff} calculations for thin HRES clouds (Figure 2c) show that the obtained LRES r_{eff} will be close to the climatological value of 8 μm for cloud fractions < 0.4 because the LRES τ values for these fractions are smaller than 4 (see Figure 2a). At these low optical thickness values, the relative contribution of the climatological value is > 50%. Further, for cloud fractions between 0.5 and 0.9 the LRES r_{eff} is larger over a dark than over a bright surface. This is explained by the fact that a cloud-free HRES pixel over a dark surface decreases the LRES 1.6-μm reflectance more than a bright surface does. Because r_{eff} is inversely proportional to the 1.6-μm reflectance, this leads to a larger r_{eff} over a dark surface.

Figure 2d shows that for HRES clouds with τ =20 and r_{eff}=16 μm the LRES r_{eff} is still considerably relaxed to the climatological value of 8 μm for cloud fractions below 0.2. For cloud fractions between 0.4 and 0.7 the LRES r_{eff} over a dark surface approaches 24 μm, which is the maximum r_{eff} value that is considered for water clouds. In these cases it is likely that cloud phase “ice” instead of “water” will be assigned to the LRES clouds when the cloud-phase retrieval would be solely based on the 0.6-μm and 1.6-μm reflectance. However, due to the cloud-top temperature test, a part of these clouds will still be labelled as “water”. The simulations show that a shift from phase “water” to “ice” can occur over both ocean and land surfaces, but will occur more often over darker than over bright surfaces.

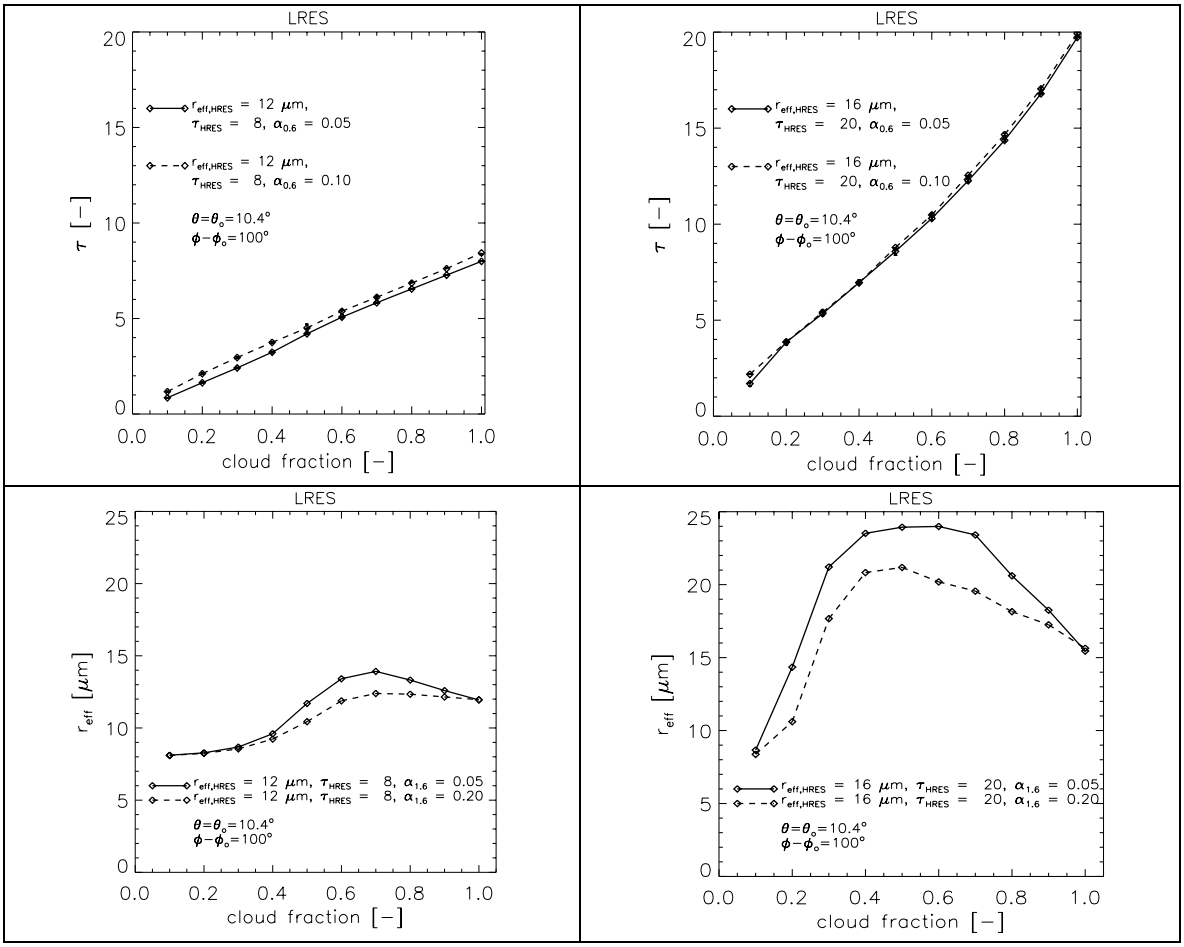

Figure 2: **Simulated LRES τ (upper panels) and r_{eff} (lower panels) as function of cloud fraction for a water cloud with τ_{HRES} =8, $r_{eff,HRES}$=12 μm (left panels) and τ_{HRES}=20, $r_{eff,HRES}$=16 μm (right panels). Calculations were performed for a dark (ocean, $\alpha_{0.6}=\alpha_{1.6}=0.05$, solid line) and bright (mid-latitude land, $\alpha_{0.6}=0.10$, $\alpha_{1.6}=0.20$, dashed line) surface. Solar and viewing zenith angles are 10.4°, the azimuth difference angle is 100°.**

3.3. Inhomogeneous overcast cloud simulations

Figure 3 presents differences between simulated LRES and HRES particle effective radius (Δr_{eff}) for overcast inhomogeneous clouds with a cloud optical thickness distribution having a median τ value of 8 (left panel) and 15 (right panel). Because the HRES r_{eff} is fixed at 12 μm (left panel) and 16 μm (right panel), the variation seen in LRES r_{eff} is solely caused by the variation in τ. At $NIQR_\tau$=0, the overcast cloud field is homogeneous and all HRES τ values are 8 and 15 in Figure 3a and 3b, respectively. The simulated LRES r_{eff} values diverge from their HRES counterparts with increasing inhomogeneity for both cloud optical thickness distributions, with larger differences over a dark ($\Delta r_{eff}\approx$4 μm at $NIQR_\tau$=1.5) than over a bright surface ($\Delta r_{eff}\approx$2 μm at $NIQR_\tau$=1.5). This is explained by more contrast between the cloudy reflectance of a semi-transparent cloud and the reflectance of the underlying dark surface, thus the 1.6-μm is decreased more over a dark than over a bright surface. Note that for optically thick clouds the underlying surface is of no influence. It is evident that the LRES r_{eff} is considerably overestimated for overcast fields of inhomogeneous water clouds. The results shown here are in agreement with findings of Deneke et al. (2007), who showed that low-resolution r_{eff} is overestimated by 1-2 μm compared to high-resolution. Similar to the results of the broken cloud fields, increased cloud inhomogeneity may lead to shifts from phase “water” to phase “ice”, is more likely to occur over dark than over bright surfaces and is dependent on the HRES r_{eff}.

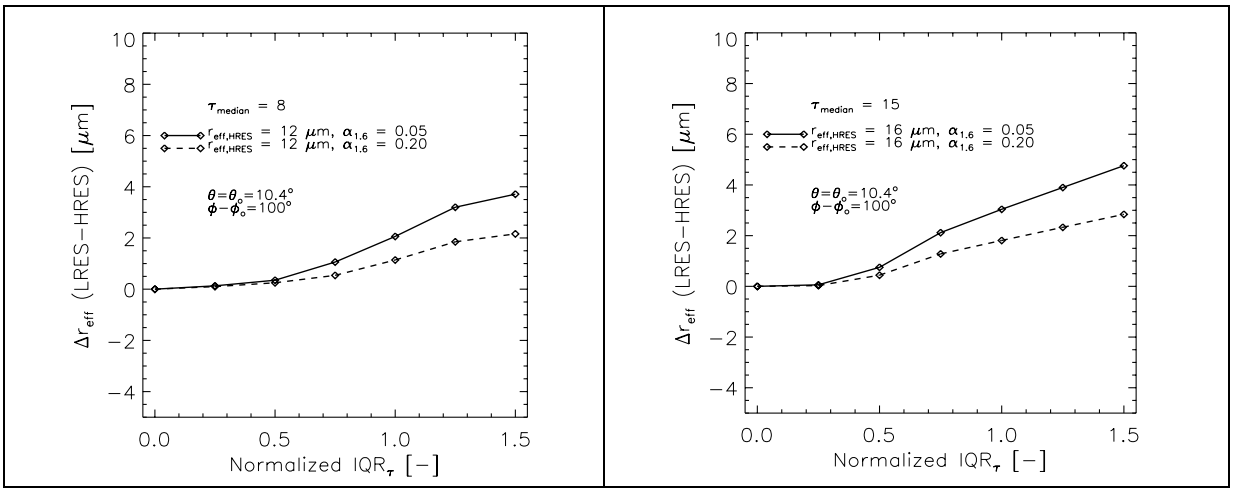

Figure 3: **Simulated difference in obtained effective radius (Δr_{eff}) between LRES and HRES for overcast water clouds as function of cloud inhomogeneity expressed as Normalized Interquartile Range (NIQR) of τ (see text for its definition). Results are shown for a dark (solid line) and bright surface (dashed line) for clouds with HRES τ_{median}=8 (left panel) and τ_{median}=15 (right panel). Values for HRES r_{eff} were fixed at 12 μm (left panel) and 16 μm (right panel).**

3.4 MODIS observations

Figure 4a shows the observed mean LRES r_{eff} from MODIS data over central Europe. The total number of observations over the two areas for May and August 2007 was 1353. Note that in order to asses the amount of erroneous LRES cloud-phase retrievals, only HRES assigned water clouds were considered. It can be seen that the LRES r_{eff} is higher at low cloud fractions than at high cloud fractions, which indicates that the cloud-free HRES pixel reflectances have some influence on the LRES r_{eff} retrieval. The upper limit of the standard deviation is 14 μm at maximum, which indicates that r_{eff} values will scarcely approach 24 μm. The LRES r_{eff} gradually decreases to about 10 μm when clouds are less fractional.

Figure 4b shows the difference between LRES and HRES retrieved r_{eff} from MODIS data. Over central Europe the difference increases to +2 μm at NIQR between 1.0 and 1.5. Figures 4a indicates that in reality the effect of broken clouds is less than obtained from the synthetic datasets. For these clouds, it may be due to the smaller HRES τ than compared to the synthetic fields. Furthermore, the broken cloud fields from the MODIS observations vary in both HRES τ and r_{eff}, while the synthetic broken cloud fields were ingested with constant values of τ and r_{eff}.

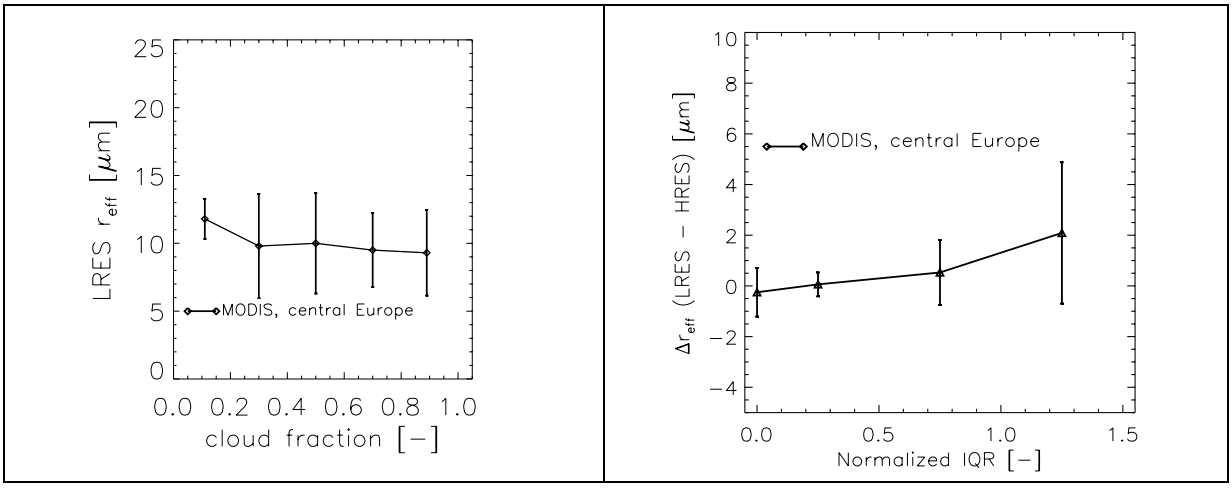

Figure 4: a) MODIS mean LRES r_{eff} retrievals over central Europe, with error bars indicating the standard deviation. Only results for HRES indicated water clouds with τ > 4 are shown, binsize = 0.2, b) MODIS LRES – HRES r_{eff} for overcast clouds, binned for each 0.5 NIQR unit and plotted at the respective bin centers. Error bars denote the standard deviation of the differences. Results are shown for HRES water clouds.

Finally, it is mentioned again that we did not account for 3D cloud effects in our simulations. Although we restricted solar and viewing angles to within 60^o, the MODIS observations may be influenced by 3D effects.
The total effect on the cloud-phase retrieval is only marginal for the data investigated. We found that less than 1% of the HRES assigned water clouds switch from water at HRES to "ice" at LRES. Further investigation is required to fully assess the broken cloud and cloud inhomogeneity effect for the entire suite of cloud physical properties obtained from visible and near-infrared reflectances (τ, r_{eff}, LWP, and CPH).

4 SUMMARY AND CONCLUSIONS

To assess the impact of broken cloudiness and inhomogeneous clouds on satellite cloud-phase retrievals, simulations for the two effects were made. Synthetic broken cloud fields were made by mixing high-resolution fields of constant τ and r_{eff} with a certain degree of high-resolution cloud free pixels. After averaging the 0.6- and 1.6-μm reflectance, the low-resolution τ and r_{eff} were obtained. For cloud fractions $\approx$0.4-0.8, dependent on the high-resolution cloud optical thickness, effective radius, and the underlying surface the low-resolution effective radius is overestimated. This overestimation is related to the darkening effect of the high-resolution cloud-free reflectances.
Synthetic overcast, inhomogeneous clouds were obtained by fixing r_{eff} and imposed variation in τ. The calculations reveal that the overestimation of low-resolution r_{eff} increases with increasing inhomogeneity, which is due to the fact that although r_{eff} is fixed, the variation in τ causes not only a decrease in the low-resolution averaged 0.6-μm reflectance, but also a decrease in the averaged 1.6-μm reflectance. As a result, the low-resolution r_{eff} is larger than the high-resolution counterpart. Further, the overestimation is larger over a dark surface, which is probably owing to the surface albedo contribution in case of semi-transparent clouds, which causes an additional darkening of the low-resolution 1.6-μm reflectance.
The MODIS observations for broken clouds and inhomogeneous overcast cloud fields reveal that r_{eff} is indeed overestimated at low cloud fractions and large inhomogeneity, however, the effect is much less than expected from the synthetic data. Differences between the synthetic datasets and MODIS retrievals are likely due to more variation in both τ and r_{eff} in reality than in the synthetic data and 3D cloud effects, which were not accounted for in the simulations.
The overall influence of broken clouds and inhomogeneous overcast clouds was found to be very small for the dataset investigated. Less than 1% of the high-resolution assigned water clouds were labelled "ice" at low-resolution. We suggest that the additional cloud-top temperature check prevents for more erroneous low-resolution cloud-phase retrievals. This needs to be confirmed by additional research.

ACKNOWLEDGMENTS

This work was performed within the EUMETSAT funded Climate Monitoring Satellite Application Facility (CM-SAF). MODIS Level-1 and -2 data were downloaded from the Level-1 and Atmosphere Archive and Distribution System (LAADS). MODIS surface albedo files were obtained using the Land Process Distributed Active Archive Center (LP-DAAC).

REFERENCES

De Haan, J. F., P. B. Bosma, and J. W. Hovenier, The adding method for multiple scattering calculations of polarized light, Astron. & Astrophys., **183**, 371–391, 1987.

Deneke, H.M., R.A. Roebeling, E.L.A. Wolters, and A.J. Feijt, Intercomparison of cloud properties derived from MODIS and METEOSAT-SEVIRI, Conf. Proc. AGU Fall Meeting, San Francisco, CA, USA, 2007.

Frey, R. A., S. A. Ackerman, Y. Liu, K. I. Strabala, H. Zhang, J. R. Key, and X. Wang, Cloud detection with MODIS, part I: Improvements in the MODIS cloud mask for collection 5, J. Atmos. Ocean.

Technol., **25**, 1057–1072, 2008.

Hess, M. R.B.A. Koelemeijer, and P. Stammes, Scattering matrices of imperfect hexagonal ice crystals, J. Quant. Spectrosc. Radiat. Transfer, **60**, 301-308, 1998.

Minnis, P., D.P. Gardner, D.F. Young, R.F. Arduini, and Y. Takano, Parameterizations of reflectance and effective emmitance for satellite remote sensing of cloud properties, J. Atmos. Sci., **55**, 3313-3339, 1998.

Nakajima, T., and M. D. King, Determination of the optical thickness and effective particle radius of clouds from reflected solar radiation measurements, part 1: Theory, J. Atmos. Sci., **47**, 1878-1893, 1990.

Roebeling, R. A., A. J. Feijt, and P. Stammes, Cloud property retrievals for climate monitoring: Implications of differences between Spinning Enhanced Visible and Infrared Imager (SEVIRI) on METEOSAT-8 and Advanced Very High Resolution Radiometer (AVHRR) on NOAA-17, J. Geophys. Res., **111**, 2006.

Roebeling, R. A., H. M. Deneke, and A. J. Feijt, Validation of Cloud Liquid Water Path Retrievals from SEVIRI Using One Year of CloudNET Observations, J. Appl. Meteor. Climatol. 47 , 206–222, 2008.

Schulz, J. and Coauthors, Operational climate monitoring from space: the EUMETSAT Satellite Application Facility on Climate Monitoring (CM-SAF), Atmos. Chem. Phys. Disc., **8**, 8517–8563, 2008.

Stammes, P., Spectral radiance modelling in the UV-Visible range, in IRS 2000: Current problems in Atmospheric Radiation, edited by W. L. Smith and Y. M. Timofeyev, pp. 385–388, A. Deepak, Hampton, VA, 2001.

Wolters, E. L. A., R. A. Roebeling, and A. J. Feijt, Evaluation of cloud phase retrieval methods for SEVIRI onboard Meteosat-8 using ground-based lidar and cloud radar data, J. Appl. Meteor. Climatol., **47**, 1723–1738, 2008.